



## ISTITUTO NAZIONALE DI RICERCA METROLOGICA Repository Istituzionale

The effect of cobalt doping on the efficiency of semiconductor oxides in the photocatalytic water remediation

*Original*

The effect of cobalt doping on the efficiency of semiconductor oxides in the photocatalytic water remediation / Gonçalves, Nuno P. F.; Paganini, Maria Cristina; Armillotta, Paolo; Cerrato, Erik; Calza, Paola. - In: JOURNAL OF ENVIRONMENTAL CHEMICAL ENGINEERING. - ISSN 2213-3437. - 7:6(2019), pp. 1034751-1034759. [10.1016/j.jece.2019.103475]

*Availability:*

This version is available at: 11696/82859 since: 2025-01-16T13:27:37Z

*Publisher:*

Elsevier

*Published*

DOI:10.1016/j.jece.2019.103475

*Terms of use:*

This article is made available under terms and conditions as specified in the corresponding bibliographic description in the repository

*Publisher copyright*

(Article begins on next page)



# The effect of cobalt doping on the efficiency of semiconductor oxides in the photocatalytic water remediation

Nuno P.F. Gonçalves, Maria Cristina Paganini\*, Paolo Armillotta, Erik Cerrato, Paola Calza\*

Department of Chemistry, Università di Torino, Torino, Italy

## ARTICLE INFO

### Keywords:

Oxide materials  
Semiconductors  
Cobalt doping  
Heterogeneous photocatalysis  
Water treatment

## ABSTRACT

The effect of cobalt doping on semiconductor materials synthesized *via* solution and hydrothermal methods was investigated by testing its photocatalytic efficiency on pollutants abatement. X Ray Diffraction technique was used to evaluate samples crystallographic phases allowing to identify different species due to the introduction of the dopants. Diffuse Reflectance UV–vis Spectroscopy was employed to determine the bandgap as well as the absorption corresponding to d-d transitions for cobalt doped systems. Finally, Electron Paramagnetic Resonance Spectroscopy was adopted to perform a pre-screening of the photoactivity of the prepared samples.

The Co-doped TiO<sub>2</sub> and ZnO materials photoactivity was assessed on phenol degradation, selected as pollutant probe, under UVA irradiation. Doping TiO<sub>2</sub> with cobalt in low amounts (0.25% and 0.5%) prepared by hydrothermal method leads to an enhancement on phenol degradation. Also, the presence of Co-doped ZnO obtained by hydrothermal process if prepared with defined cobalt amount (0.5 or 1%) promote an increasing on phenol abatement. Ketoprofen was used to evaluate the doping effect, being the Co-doped ZnO material more efficient on ketoprofen mineralization comparing with bare material. The ketoprofen and its transformation products were easily abated and, in wastewater, they were completely eliminated within 1 h, endorsing that inserting cobalt can improve the ZnO photocatalysis efficiency for water remediation.

## 1. Introduction

Water pollution has emerged as a global critical concern. The occurrence of pollutants has been increasingly detected at low concentrations levels in surface water, groundwater and drinking water [1,2]. Particular attention should be paid to contaminants of emerging concern (CECs) such as pharmaceuticals, personal care products, artificial sweeteners and pesticides that, due to their toxicity, even at low levels, may have a negative impact on ecosystems including human beings [3,4]. Considerable efforts have been recently dedicated to developing new solutions to improve the wastewater treatment systems efficiency removing those pollutants [5–8].

Heterogeneous photocatalytic has become one of the most promising solutions for environmental remediation due to its ability to generate highly reactive oxidizing species able to remove a wide range of contaminants [9]. Among the semiconductors, titanium dioxide [10,11] and zinc oxide [12,13], thanks to their chemical and physical high stability, broad adsorption range, high electronic coupling coefficient and photo-stability, has been widely reported as the leading candidates.

The introduction of doping agents is described as a successful

approach to improve the semiconductor photocatalytic efficiency. The addition of supplementary energy levels on the oxide bandgap, can potentially act as a charger trap, reducing the recombination of the photogenerated electrons/holes allowing carries to successful diffuse to the surface resulting in better photocatalytic activity [14–16]. Conversely, the introduction of doping agents can also form a charger recombination center into the system lattice [17,18]. Among dopants, d block metals can configure some stability reducing the photo-corrosion limitations of semiconductors oxides [17,19]. Additionally, transition metals can modify the semiconductor lattice, inducing reticular distortions increasing the fraction defects that can lead to higher efficiency in the electron holes charges separation [14,20]. The incorporation of transition metal ions in oxides semiconductors appears to be a complex function of dopant concentration and its distribution, strongly dependent on each metal ion electron donor density and its d electron configuration.

Cobalt is considered one of the most effective doping species due to its abundant electronic states and also it appears to suite well for tailoring the electronic structure, by substitution of Co<sup>2+</sup> on the host lattice without inducing significant distortions in the oxide reticulum [21,22]. In addition, the incorporation of cobalt ions has shown an

\* Corresponding authors.

E-mail addresses: [mariacristina.paganini@unito.it](mailto:mariacristina.paganini@unito.it) (M.C. Paganini), [paola.calza@unito.it](mailto:paola.calza@unito.it) (P. Calza).

<https://doi.org/10.1016/j.jece.2019.103475>

Received 11 July 2019; Received in revised form 7 October 2019; Accepted 11 October 2019

Available online 19 October 2019

2213-3437/ © 2019 The Authors. Published by Elsevier Ltd. This is an open access article under the CC BY license (<http://creativecommons.org/licenses/by/4.0/>).

increase in the number of oxygen vacancies in the ZnO structure that are usually leading to an efficient separation of photogenerated charges carriers [23,24]. However, the introduction of cobalt with different concentrations on ZnO lattice is reported to induce a change in the morphology on the microstructures suggesting that structure and activity strongly depend on the synthesis method [25].

The novelty of this work consists both in the use of ZnO and in the synthesis techniques adopted. Its properties have been studied since the early days of semiconductor electronics, but the use of ZnO as a semiconductor in photocatalysis has been hindered by the lack of control over its electronic structure: ZnO crystals are almost always n-type, the cause of which has been a matter of extensive debate and research. Theoretical studies have also contributed to a deeper understanding of the role of native point defects and impurities on the unintentional n-type conductivity in ZnO. Band-gap engineering of ZnO can be achieved by alloying with dopants and Co in particular can suit for photocatalytic purpose. It has been also demonstrated that the synthesis procedure can dramatically influence the morphology of the final sample and consequently the surface area and the photocatalytic properties

In the present work, a comprehensive investigation of the cobalt doping role on different newly semiconductors oxide materials, produced through different synthetic methods, correlating the reticular structure with their photocatalytic activity for removal of pollutant from water. The Co-doping concentration effect (from 0.25 to 5%), as well as the synthesis procedure (solution and hydrothermal methods), are assessed on the TiO<sub>2</sub> and ZnO photocatalytic efficiency for phenol abatement, used as pollutant model molecule due to its chemical structure. The efficiency of the most promising material was also evaluated on ketoprofen degradation, a contaminant of emerging concern that have been detected in natural waters with concentrations of ng/L [26,27].

## 2. Materials and methods

### 2.1. Materials

All chemicals used in this work were obtained from Sigma-Aldrich. The real wastewater samples used in this study were collected on a Waste Water Treatment Plant on northwest area of Italy (October 27<sup>th</sup> 2017) from the outflow of primary clarifier tank. Samples were filtered using a Whatman grade qualitative filter paper before filtering with a 0.45 µm filter Sartolon Polyamide (Sartorius Biolab). Wastewater analyses allowed to determine a total organic carbon concentration of 9.7 mg/L; 68.4 mg/L of inorganic carbon; 31.3 mg/L of total nitrogen and pH value of 8.3.

### 2.2. Materials synthesis

Bare and cobalt doped photocatalysts were prepared *via* solution (S) and hydrothermal method (H) [28,29]. Samples were obtained with different nominal amount of Cobalt (0.25, 0.5, 1, 3 and 5% molar), labelled respectively Co(0.25%)-ZnO, Co(0.5%)-ZnO, Co(1%)-ZnO, Co(3%)-ZnO, and Co(5%)-ZnO for the zinc oxide materials. The corresponding titanium dioxide materials were labelled Co(0.25%)-TiO<sub>2</sub>, Co(0.5%)-TiO<sub>2</sub>, Co(1%)-TiO<sub>2</sub>, Co(3%)-TiO<sub>2</sub>, and Co-(5%)-TiO<sub>2</sub>.

#### 2.2.1. Synthesis via solution method (S) for ZnO and TiO<sub>2</sub>

ZnO materials were synthesized dissolving 2.2 g of Zn(CH<sub>3</sub>COO)<sub>2</sub> in 160 mL of water and 80 mL of ethanol. The stoichiometric amount of Co(NO<sub>3</sub>)<sub>2</sub>·6H<sub>2</sub>O was added to obtain the doped samples. The mixture was kept under magnetic stirring for 1 h in order to promote the solubilization of organic salts. Then, a proper dose of NaOH 1 M was added dropwise to the solution in order to reach a pH of 10–11. The obtained gel was left to rest for two days and then dried in an oven at 70 °C. The powder was finally calcined at 300 °C for 30 h.

TiO<sub>2</sub> was prepared from 7.5 mL of titanium isopropoxide (97% wt)

dissolved in 2-propanol (7.5 mL) and deionized water (4 mL; the desired stoichiometric amount of (Co(NO<sub>3</sub>)<sub>2</sub>·6H<sub>2</sub>O) was added to the solution together with 5 g of citric acid. The solution was subjected to magnetic stirring and kept for 6 h in a hot water bath at 80 °C, in order to favor the gel formation [30]. The acidic pH favored the hydrolysis process and therefore the gelation. The sample was placed in an oven at 70 °C for two days, in order to promote drying and obtaining the xerogel. This phase was followed by a further heat treatment which involved calcining in a muffle at 500 °C for 2 h obtaining a light-yellow powder.

#### 2.2.2. Synthesis via hydrothermal method (H) for ZnO and TiO<sub>2</sub>

To obtain Co-doped ZnO, the Co(NO<sub>3</sub>)<sub>2</sub>·6H<sub>2</sub>O, in the desired percentage, was added to 20 mL of Zn(NO<sub>3</sub>)<sub>2</sub>·6H<sub>2</sub>O 1 M solution, and the resulted solution was kept under stirring. After complete dissolution, a solution of NaOH 4 M was added dropwise until reaching the pH value of 10. The solution was transferred to a 100 mL Teflon-lined autoclave, filled with water until complete 50 mL, and the autoclave was kept at 175 °C for 15 h. The resulting precipitated products were washed with water and recovered by centrifugation (6000 rpm for 10 min), repeating the procedure 2 times. After dried at 70 °C during the night, the powders were homogenized using a mortar and pestle.

The same procedure was used to obtain Co-doped TiO<sub>2</sub>; also in this case the cobalt precursor (Co(NO<sub>3</sub>)<sub>2</sub>·6H<sub>2</sub>O) was added to titanium(IV) butoxide (3.35 mL) and ethanol (50 mL). The solution was kept under continuous stirring for 10 min at room temperature. Then, 0.2 mL of sulfuric acid 98% and 0.2 mL of water were added at the starting solution. The thermal treatment was the same used for ZnO materials.

### 2.3. Methods

X-ray powder diffraction (XRPD) analyses were performed in a PANalytical X'Pert PRO, (45 kV, 40 mA) using Cu as radiation source. Analyses were performed continuously in the 2θ range between 10° and 100°. The X'Pert High-Score software was used for the mineral phases identification. The UV–vis absorption spectra were recorded using a Varian Cary-5000 spectrophotometer, coupled with an integration sphere for diffuse reflectance studies (DRS), and a PTFE sample as reference using a Cary WinUV software. The Electron Paramagnetic Resonance analyses were performed in a X-band CW-EPR Bruker EMX spectrometer equipped with a cylindrical cavity operating at 100 KHz field modulation, in both at room temperature and at liquid N<sub>2</sub> temperature (77 K).

#### 2.3.1. Photocatalytic degradation procedure

The photocatalytic experiments were performed in Pyrex glass cells containing 5 mL solution at room temperature under magnetic stirring. The initial concentration of pollutant molecule was 20 mg/L in the presence of 1000 mg/L of catalyst. Irradiation was performed using a Philips Cleo 6 × 15 W TL-D Actinic BL (290–400 nm range, 90 ± 2 Wm<sup>-2</sup>) with emission max. at 365 nm, measured with a CO.FO.ME.GRA power meter. Before the analysis, to remove the heterogeneous catalyst, the samples were filtered using a 0.45 µm filter. Experiments in wastewater samples were conducted after spiked with phenol and ketoprofen.

#### 2.3.2. Analysis

The samples were analyzed using a YL9300 HPLC system equipped with a column, LiChroCART, 12.5 cm x 0.4 cm; 5 m (Merck). Phenol concentration was determined using as eluent acetonitrile/phosphoric acid solution (1 × 10<sup>-2</sup> M) at pH 2.8 (10:90%, v:v); 1 mL/min and detector at 220 nm. Ketoprofen was followed with the same eluent in a mixture of 35: 65% v:v, at 260 nm.

HPLC/MS analyses were performed in a Shimadzu UFLC with a Nexera XR, a pump LC-20AD XR, SPD-M20A UV/vis detector and SCIEX QTrap A3200. Data were acquired in full-scan mode in a range between 50–300 m/z in ESI negative mode. Using Luna C18 50 x 2 mm, 2.5 µm

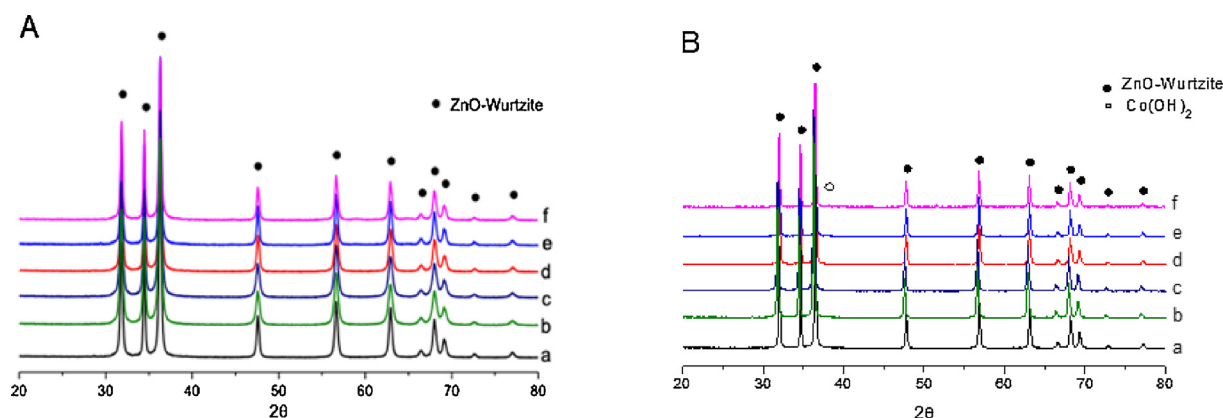


Fig. 1. Diffratograms of bare and Co-ZnO prepared via (A) solution and (B) hydrothermal methods, a) pristine ZnO, b) Co(0.25%)-ZnO, c) Co(0.5%)-ZnO, d) Co(1%)-ZnO, e) Co(3%)-ZnO, f) Co(5%)-ZnO.

(Phenomenex) column at flow rate 0.4 mL/min and the eluent gradient acetonitrile/water (v/v): 5/95 (0 min); 0/100 (5 min); 0/100 (5 min).

Total organic carbon (TOC) and total nitrogen (TN) was quantified with Shimadzu TOC-5000 analyzer using standards of potassium phthalate for the calibration.

### 3. Results and discussion

#### 3.1. Materials characterization

Fig. 1 shows the diffractograms of pristine zinc oxide and zinc oxide doped with cobalt at different concentrations, prepared by solution (A) or hydrothermal methods (B). The XRD patterns of the synthesized samples display reflections corresponding to (1 0 1), (0 0 2), (1 0 1), (1 0 2), (1 1 0), (1 0 3), (2 0 0), (1 1 2) and (2 0 1) planes of the ZnO wurtzitic hexagonal phase. No other reflections were recorded, suggesting the high purity of the synthesized samples; in addition, the diffraction peaks are relatively sharp, indicating the good crystallinity of the materials.

The doping with cobalt does not modify the diffraction profile of zinc oxide, corroborating the hypothesis that the doping species were able to effectively enter the crystalline lattice of the solid and substitute itself with the zinc atoms. The good dispersion of the cobalt ions in the crystalline lattice of the oxide or the small fraction of dopant addition prevents observing signals referable to other crystalline phases, such as the cubic spinel form of  $\text{Co}_3\text{O}_4$ . In fact, all the diffraction patterns were characterized by the same reflections at the same value of  $2\theta$ . This experimental evidence suggests that, independently of the synthesis method, cobalt doping does not modify the wurtzite structure typical of zinc oxide.

For a more in-depth analysis an enlargement of the diffraction profiles in the region  $30^\circ < 2\theta < 40^\circ$  are shown in Figure S1 where the most intense reflections fall. The peaks retain their position, with a negligible displacement at greater angles as the concentration of cobalt increases. This effect can be explained by considering the very slightly different values of the ionic radii of  $\text{Co}^{2+}$  ( $r_{\text{Co}^{2+}} = 0.070$  nm) and of the  $\text{Zn}^{2+}$  ( $r_{\text{Zn}^{2+}} = 0.074$  nm). The interstitial ions, having almost the same size than those of zinc, generate a very small disorder and negligible stress in the crystalline structure of the oxide. Furthermore, the signals of pristine zinc oxide appear more intense and narrower than the reflections of cobalt-containing powders. The peaks enlargement is more evident at higher dopant concentrations. The signal amplitude is a parameter related to the degree of crystallinity of the sample; the increase in the percentage of doping inhibits, therefore, the crystallization and limits the growth of the crystallites.

The Scherrer equation on XRD pattern reported below, was used to evaluate the size of the average crystals of synthesized materials [31]:

$$\tau = \frac{K\lambda}{\beta \cos \theta}$$

where  $\tau$  is the mean size of the ordered crystalline domain,  $K$  is a dimensionless shape factor which varies varying the nanoparticles morphology and in this case we used a value of 0.9 which is suitable for platelet shape [32],  $\lambda$  is the X-ray radiation wavelength,  $\beta$  is line broadening at half maximum intensity (FWHM) after subtracting the instrumental line broadening which in our case were performed with a silicon single-crystal standard and  $\theta$  is the Bragg angle at which we measure the reflection.

Generally, the increasing of cobalt percentage in the matrix affects the degree of crystallinity and consequently the reduction in the crystallites dimensions, but in the case of  $\text{TiO}_2$  obtained via hydrothermal synthesis, this phenomenon does not occur (Table 1). By comparing these values, it is possible to state that the hydrothermal synthesis ensures a greater degree of crystallinity of the powders only in the case of ZnO (see figure S1 where it is possible to compare different width). Also, in the case of  $\text{TiO}_2$ , the XRD analysis (Fig. 2) reveals the formation of a single phase corresponding to anatase structure. No influence of Co-doping is observable in the XRD patterns, in fact, it is not possible to identify the presence of cobalt-like phases like the spinel cobalt oxide, or cobalt hydroxide. Regardless of the synthesis procedure and the type of transition metal added, all the materials show the same diffraction profile and this is compatible with what is reported in the literature [33–35]. In the case of titania type of synthesis performed does not affect the degree of crystallinity of the sample and consequently the size of the nanoparticles as reported in Table 1.

Also, for  $\text{TiO}_2$  samples an enlargement of the diffraction profiles in the region  $20^\circ < 2\theta < 30^\circ$  is shown in Figure S2 where the most intense reflections fall. Both the synthesis procedures bring to the formation of pure anatase, moreover, it is possible to observe a slight enlargement of the peaks related to the doped materials respect to the pure ones. This phenomenon is particularly evident for the samples prepared via hydrothermal methods (see figure S2).

In DR-UV-vis spectra for all the samples Co-ZnO (Fig. 3, Panel A and

Table 1

Average size of crystallites (d), for pure and doped materials.

% Co	d (nm) for ZnO		d (nm) for $\text{TiO}_2$	
	S	H	S	H
0	37 ± 5	143 ± 30	8 ± 2	4 ± 1
0.25	36 ± 6	141 ± 20	7 ± 2	5 ± 2
0.5	34 ± 5	141 ± 17	6 ± 2	6 ± 2
1	32 ± 7	140 ± 18	6 ± 2	5 ± 2
3	30 ± 6	125 ± 14	6 ± 2	8 ± 2
5	35 ± 7	116 ± 17	6 ± 2	4 ± 1

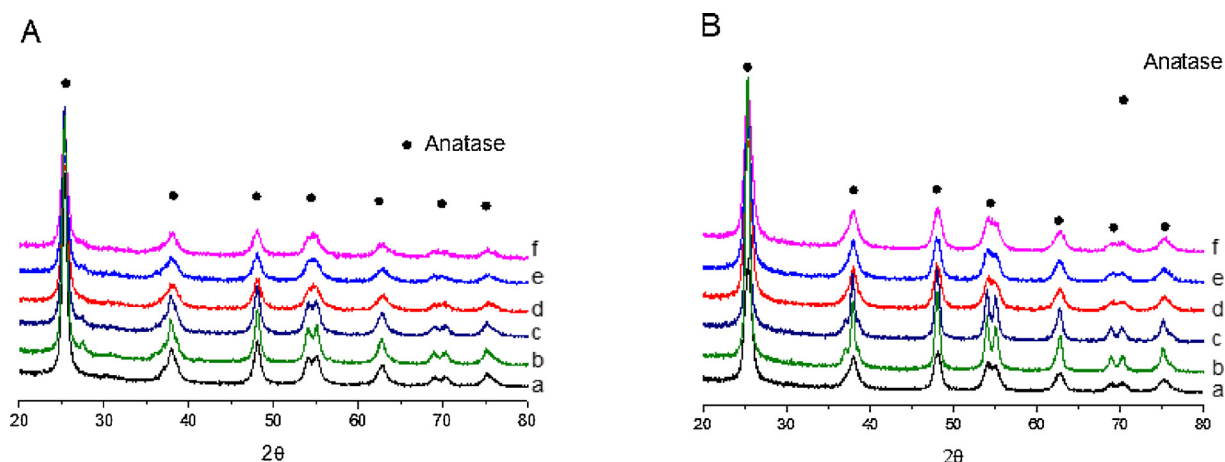


**Fig. 2.** Diffractograms of bare and Co-TiO<sub>2</sub> prepared via (A) solution and (B) hydrothermal methods; a) bare TiO<sub>2</sub>, b) Co(0.25%)-TiO<sub>2</sub>, c) Co(0.5%)-TiO<sub>2</sub>, d) Co(1%)-TiO<sub>2</sub>, e) Co(3%)-TiO<sub>2</sub>, f) Co(5%)-TiO<sub>2</sub>.

B) and Co-TiO<sub>2</sub> (Fig. 3, Panel C and D) obtained via solution and hydrothermal methods are shown. For all the samples the type of synthesis does not modify the optical behaviour of the semiconductor. For all the ZnO samples the band gap (calculated with the Tauc plot method) is around 3.3 eV while for titania is slightly higher about 3.4 eV. The EBG values present once again that the addition of the doping agent has no effect in defining the extent of the solid bandwidth. The presence of cobalt in the crystalline oxide lattice is confirmed by the presence in the spectrum of characteristic bands related to the d-d transitions. In the

first two panels (A and B) related to the ZnO material the presence of well-defined bands centred at 554 nm, 587 nm and 635 nm are assigned to the d-d transitions of Co<sup>2+</sup> involving crystal fields levels in a tetrahedral crystal symmetry and can be ascribed to the (F) → <sup>2</sup>E(G), <sup>4</sup>A<sub>2</sub>(F) → <sup>4</sup>T<sub>1</sub>(P) and <sup>4</sup>A<sub>2</sub>(F) → <sup>2</sup>A<sub>1</sub>(G) transitions respectively, where A, E and T are generally used to indicate intermediate energy bands [36–39]. These results support the fact that high spin tetrahedrally coordinated Co<sup>2+</sup> ions (3d<sup>7</sup>, S = 3/2) can replace Zn<sup>2+</sup> sites in the ZnO structure. With regard to these absorption bands, there is a substantial difference,

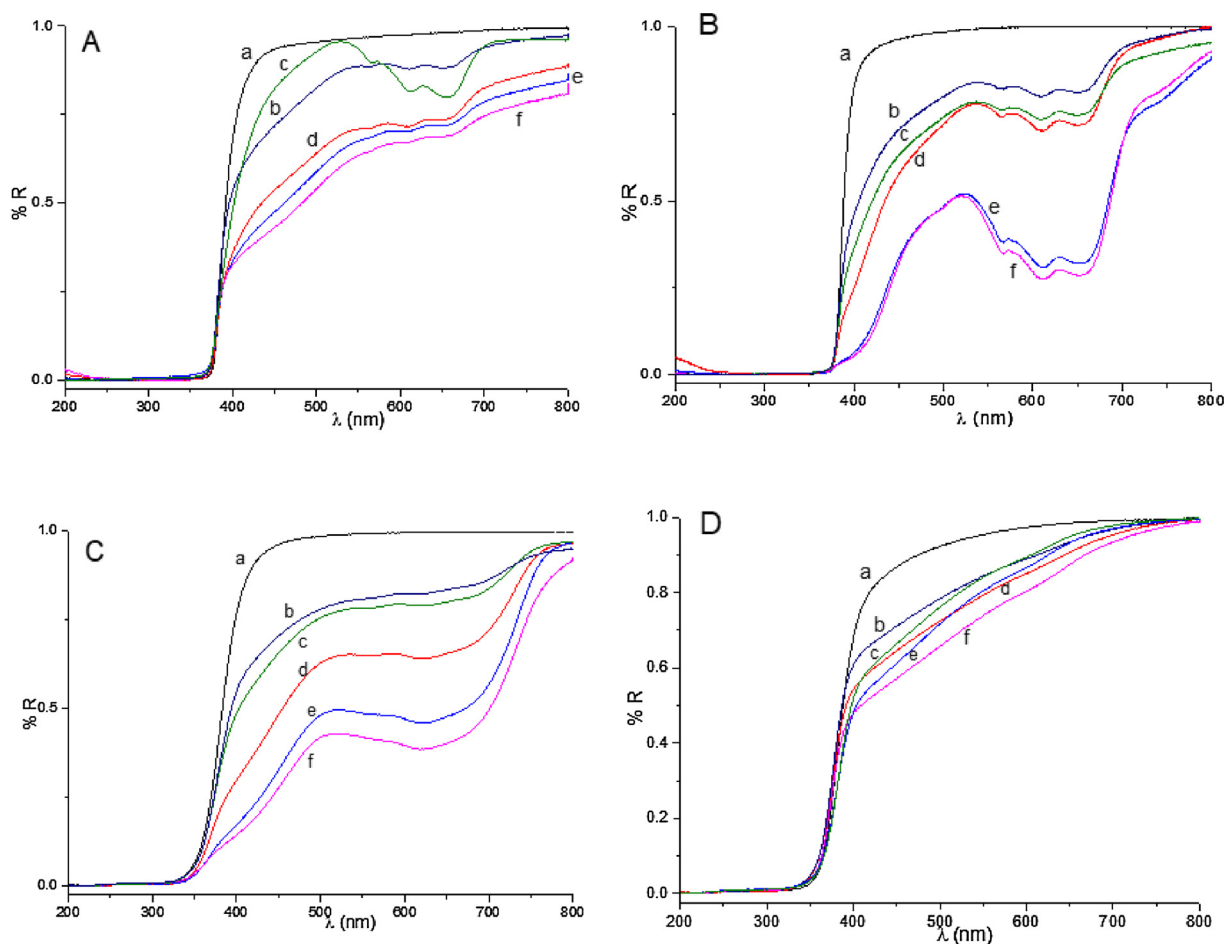


**Fig. 3.** DRS-UV-vis Reflectance spectra of A) Co-ZnO via solution synthesis, B) Co-ZnO via hydrothermal synthesis, C) Co-TiO<sub>2</sub> via solution synthesis, D) Co-TiO<sub>2</sub> via hydrothermal synthesis. a) bare ZnO, b) Co(0.25%)-ZnO, c) Co(0.5%)-ZnO, d) Co(1%)-ZnO, e) Co(3%)-ZnO, f) Co(5%)-ZnO.

especially in the intensity of these bands, for the different samples. In detail, different trends are observed for the four panels. In the case of Co-ZnO by solution method (A) the most evident aspect is the low reflectance value, the sample is in fact coloured (green) and quite dark. The d-d transitions are observed but are partially shielded by the low reflectance value. In the case of ZnO synthesized by the hydrothermal way (B) the situation is similar: indeed, again the sample with the lowest reflectance value is the one with the highest concentration of dopant, in any case, the d-d transitions are perfectly observable and well resolved. The situation for TiO<sub>2</sub> is diametrically opposed. The sample synthesized by solution method presents the absorptions due to the d-d well evident and increasing transitions as a function of the percentage of dopant (C) whereas in the case of samples synthesized by hydrothermal method (D) only the poorly defined and not resolved absorption shoulders can be observed. Also, the region of absorption is slightly different respect to the case of ZnO, in fact, the titania doped samples are yellow if obtained via hydrothermal way and pale blue if prepared via solution synthesis.

To understand the nature of the defects generated by the introduction of Co ions into the lattice of ZnO and TiO<sub>2</sub> matrices we analysed the samples with the electron paramagnetic resonance technique (EPR). The pristine oxides do not present any signals, at low magnetic field, due to paramagnetic species, this means that all the bare materials are stoichiometric and without defects. In the case of doped samples, it is possible to observe in Fig. 4A and B that the two oxides behave differently. Co-doped ZnO (Fig. 4A) presents a huge anisotropic signal: the spectrum is characterized by a strong peak centered at  $g_{\perp} = 4.5038$  and  $g_{\parallel} = 2.314$  assigned to the a  $d^7$  high spin configuration of cobalt (II) ions located in tetrahedral coordination, [33,34] replacing Zn<sup>2+</sup> sites in the wurtzitic structure. The presence of  $g_{\perp}$  and  $g_{\parallel}$  values suggest an axially distorted symmetry of the dopant into the ZnO matrix in accordance with the XRD patterns.

The signals increase with the cobalt loading (data shown in the supplementary material, Figure S4). Moreover, the lines with a g value of about 1.96 associated to shallow donors or core-shell vacancies originating from zinc, and always present in any ZnO sample, were not detected [35–37] (see Fig. 5). Another difference between doped and undoped materials is the fact in the doped ones, a consistent decrease in the signal intensities, due to native paramagnetic species is observed, as already reported by previous studies [38]. This behaviour can be explained due to cobalt in the lattice of ZnO stabilize the hexagonal structure of zinc oxide, limiting the formation of paramagnetic defects responsible for the signal around  $g \sim 1.96$ , such as the interstitial ions Zn<sup>+</sup>.

In the case of TiO<sub>2</sub> no signal related to the presence of Co<sup>2+</sup> can be observed in the same region of low magnetic field, even increasing the cobalt loading (Fig. 4B). Ti ions in titanium dioxides presents an

octahedral coordination, with tetragonal distortion; according to Liu [39] when Co ions replace Ti ions into the lattice, the charge balance and the different sizes of ionic radii of Co<sup>2+</sup> (octahedral - 0.745 Å) and Ti<sup>4+</sup> (octahedral - 0.605 Å) could easily lead to lattice distortion with the formation of defects that would reduce the stability and the crystallinity. Thus, cobalt doping could hinder the grain growth of the catalysts and reduce the particle sizes. Also, the reduced crystallinity would promote phase transformation, owing to the increased number of oxygen vacancies in the TiO<sub>2</sub> lattice created by replacing the Ti<sup>4+</sup> sites with Co<sup>2+</sup> for charge compensation. To preserve the charge balance, the formation of Ti<sup>3+</sup> species is expected. Thus, cobalt doping should enhance the concentration of Ti<sup>3+</sup> and oxygen vacancy in the lattice. The absence of this signal can be interpreted as the non-formation of the paramagnetic species due to the presence of high spin Co<sup>2+</sup> in  $d^7$  configuration. The two spectra presented in Fig. 5B are related to undoped titania (orange) and cobalt doped titania (black). The signal of Ti<sup>3+</sup> species is present only in the case of undoped TiO<sub>2</sub> and in the Co-TiO<sub>2</sub> sample it disappears; this means that probably cobalt does not enter into the titania lattice in substitutional position and it is present in a non-paramagnetic species as Co<sup>3+</sup>. Both oxides are able to trap cobalt ions in some way, the samples are coloured and different spectroscopic techniques revealed the cobalt presence but different results were obtained in the case of the two oxides, at least in terms of the nature of the defects. This different behaviour can play a role in the different photoactivity of the two samples that we will present in the next section.

### 3.2. Photocatalytic degradation with a pollutant model molecule

The materials efficiency was evaluated using phenol as pollutant model in Milli-Q water.

#### 3.2.1. Cobalt doped TiO<sub>2</sub>

Fig. 6 shows the phenol degradation obtained under irradiation in the presence of the titanium dioxide materials doped with different cobalt concentrations prepared by the solution and hydrothermal methods compared with the respective pristine titanium dioxide material. It is possible to observe a higher activity for the materials prepared through the hydrothermal method when compared with the corresponding materials prepared by solution method.

Among Co-TiO<sub>2</sub> materials prepared by hydrothermal, those with lower cobalt concentration, namely 0.25% and 0.5% allow to achieve faster phenol degradation than the pristine TiO<sub>2</sub>. While increasing the dopant amount seems to be detrimental in the photoactivity process, as evidenced on kinetic constant values presented on Table 2. This behavior can be explained in terms of population of intraband gap states in the band gap of TiO<sub>2</sub>. It is well known from the literature [40,41] that not always the doping increases the photoactivity of the bare material,

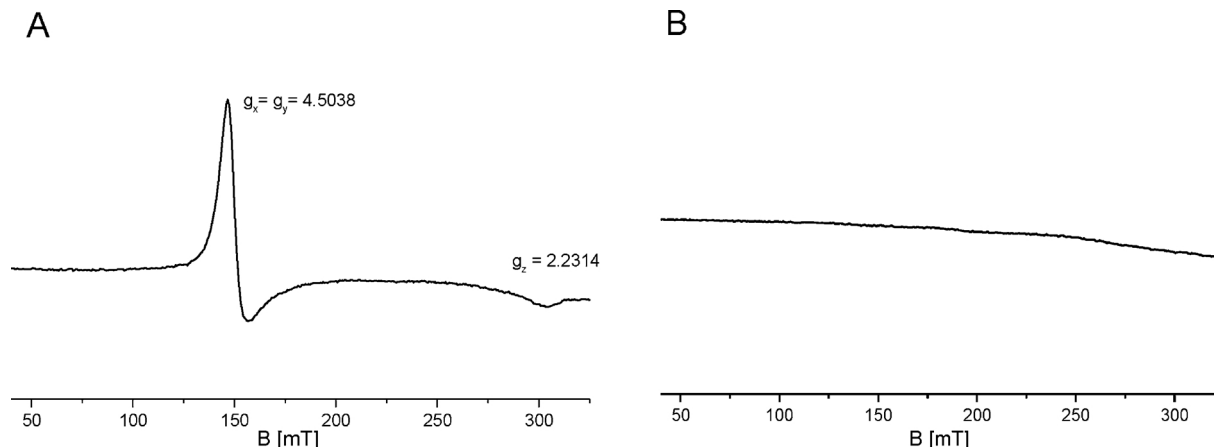


Fig. 4. EPR spectra of A) Co(1%)-ZnO via solution synthesis and B) Co(1%)-TiO<sub>2</sub> via solution synthesis.

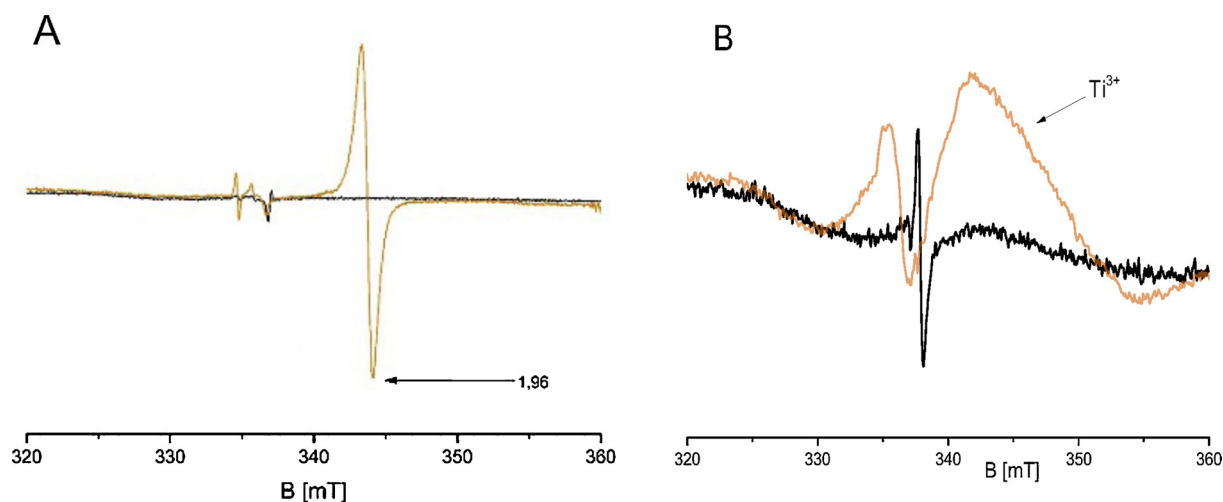


Fig. 5. Comparison of bare and cobalt doped Oxides. A) bare ZnO (orange) and Co(1%)-ZnO (black) via solution synthesis; B) bare TiO<sub>2</sub> (orange) and Co(1%)-TiO<sub>2</sub> (Black) via solution synthesis.

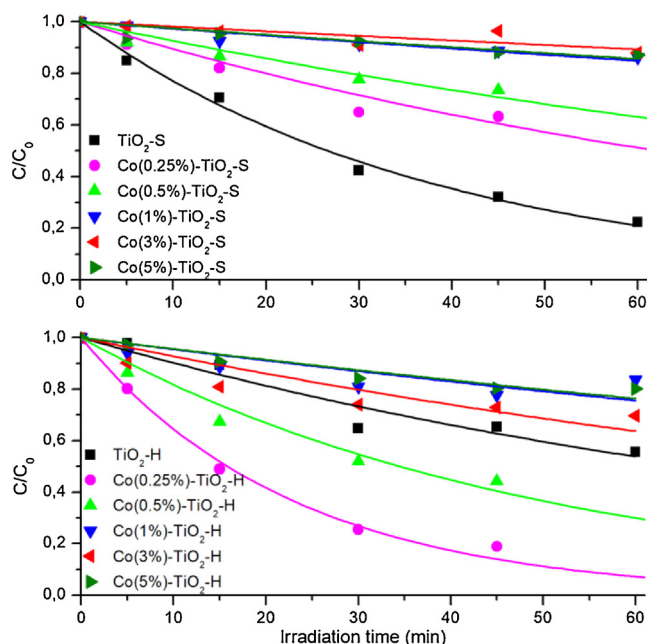


Fig. 6. Phenol degradation over time (20 mg/L) under UVA irradiation in the presence of (1000 mg/L) Co-doped TiO<sub>2</sub> prepared by solution (top) and hydrothermal method (bottom).

Table 2

Kinetic constant calculated for bare and doped materials produced through the solution and hydrothermal methods.

Material	k, min <sup>-1</sup>					
	0%	0.25%	0.5%	1%	3%	5%
TiO <sub>2</sub> -S	0.025	0.008	0.005	0.003	0.002	0.002
TiO <sub>2</sub> -H	0.010	0.028	0.013	0.006	0.001	0.005
ZnO-S	0.038	0.020	0.060	0.021	0.028	0.009
ZnO-H	0.075	0.075	0.113	0.088	0.041	0.002

it depends on the formation of recombination center into the lattice system and it is strictly related to the concentration of dopants. Most often a very low amount of extra ions leads to an increase of photocatalytic activity while an excess of dopants is detrimental. The reason, once again is related to the formation of recombination centers that

instead of helping the charge separation, brings to a faster recombination of holes and electrons. The problem of extending the spectral sensitivity of photoactive materials to visible light became one of the major challenges in applied photocatalysis and photo-electrochemistry. The simplest way to extend the spectral sensitivity ought to be the chemical modification of the materials through doping with metal cations that thus displayed additional absorption bands in the extrinsic spectral region at wavelengths longer than the absorption edge. However, such spectral extension of light absorption typically gives no improvement in integral activity of photocatalysts, since metal doping resulted in either formation of nonactive extrinsic absorption or creation of additional centers of charge carrier recombination. It depends on the coordination environment of the dopant and on its ability to modifies its oxidation number. This is the case of high concentration of cobalt (II) doping TiO<sub>2</sub>.

### 3.2.2. Cobalt doped ZnO

Fig. 7 shows the phenol degradation under irradiation in the presence of the Co-doped ZnO materials with different cobalt amounts prepared by the solution and hydrothermal methods comparing with the pristine zinc oxide. It is possible to observe a lower activity for the materials prepared through the solution method when compared with the corresponding obtained by hydrothermal method. In fact, the most active material prepared by solution method needs more than 1 h of irradiation to completely abate the model molecule, while those prepared by hydrothermal method required only 40 min. This phenomenon could be probably due to the higher degree of crystallinity of the former as pointed out by the XRD patterns. Moreover, the low calcination temperature, used for the synthesis of the ZnO obtained via solution process, does not allow a complete cleaning of the surface from the precursor. Chemically adsorbed species on the surface of the prepared material can affect the reactivity of active sites and their interaction with the pollutants.

Results obtained for the materials prepared by hydrothermal method show that cobalt doping with low concentrations induce a slight enhancement on phenol degradation when compared with the pristine ZnO, while the photoactivity is reduced as the dopant concentration increases. Actually, samples doped with 0.25%, 0.5% and 1% allow to achieve the complete phenol elimination in less than 45 min under irradiation while only 80% of the initial concentration is reduced in the presence of the material doped with 3%. For the sample prepared with the highest doping amount, namely 5%, no notably phenol degradation was observed.

As show in Table 2, the cobalt doped ZnO materials prepared via

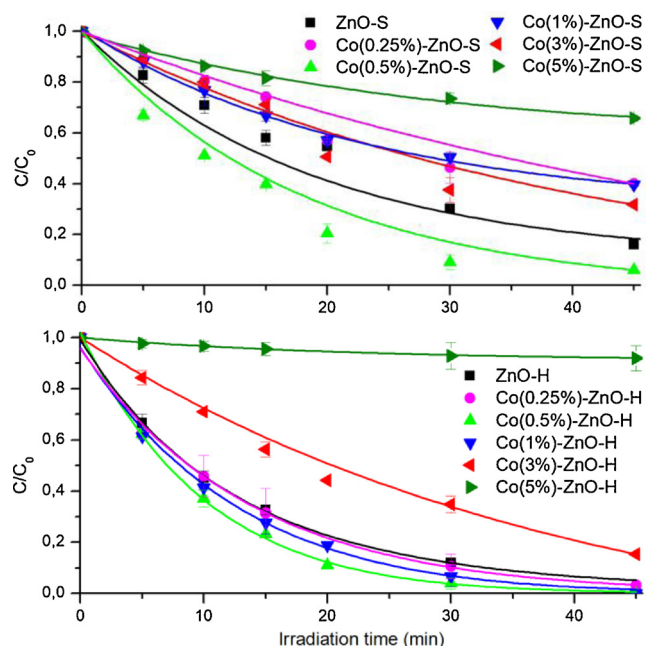


Fig. 7. Phenol degradation over time (20 mg/L) under UVA irradiation in the presence of (1000 mg/L) Co-doped ZnO prepared by solution (top) and by hydrothermal method (bottom).

hydrothermal synthesis exhibit a higher phenol degradation kinetics constant than the corresponding samples obtained by solution synthesis. These results can be explained considering that the two synthesis lead to a different sample morphology. Hydrothermal way generates more crystalline material with bigger crystals (in the case of ZnO). The photogenerated charge can be trapped by the cobalt ions, preventing the charges recombination leading to a higher charge transfer. The photogenerated charge can be trapped by the cobalt ions, preventing the charges recombination leading to a higher charge transfer [15].

According to the mechanism proposed by Ba-Abbad et al. the photocatalytic degradation ability of cobalt doped ZnO can be ascribed to the formation of reactive species in solutions like OH radicals and  $O_2^-$  due to the conversion under irradiation of  $Co^{2+}$  into  $Co^{3+}$ . The  $Co^{3+}$  ion is poorly stable and then it is easily converted into  $Co^{2+}$  [42]. This mechanism is working only with an optimal concentration of dopants, if the amount of cobalt is too high, the cobalt itself acts as recombination center for the charges.

However, the photo-efficiency for the materials containing high doping amounts, namely Co(3%)-ZnO-H and Co(5%)-ZnO-H, is reduced probably due to sufficiently high cobalt quantity to reduce the degree of crystallinity making the recombination between charges become prevalent with respect to the charge separation, which instead would have guaranteed a better functioning of the material. These results contrast with those reported by Yildirim et al. where raising the cobalt doping concentration in ZnO materials leads to a faster methylene blue degradation under visible light irradiation [43].

### 3.2.3. Phenol transformation products

The principal phenol transformation products (TPs) were followed as well, and are shown in Figure S3. The phenol TPs were identified as catechol, hydroquinone and resorcinol in agreement with those reported in the presence of  $TiO_2$  [44,45]. As observed for parent compound, the materials prepared with low concentration of cobalt allow its abatement in shorter times than those required for the pristine ZnO and Co(3%)-ZnO-H. After 45 min of irradiation, the 0.5% and 1% doped materials allow almost the complete disappearance of hydroquinone, while the pristine ZnO and 3% dopes requires 1 h of irradiation. The disappearance of resorcinol was observed with comparable slower evolution for the 3% doped ZnO.

### 3.3. Photocatalytic degradation with a CEC

The best performing material, namely Co(0.5%)-ZnO-H, was also tested on the ketoprofen degradation, that has been detected in natural waters and is reported as a contaminant of emerging concern [4,46]. Also, the ketoprofen mineralization was evaluated by determining the

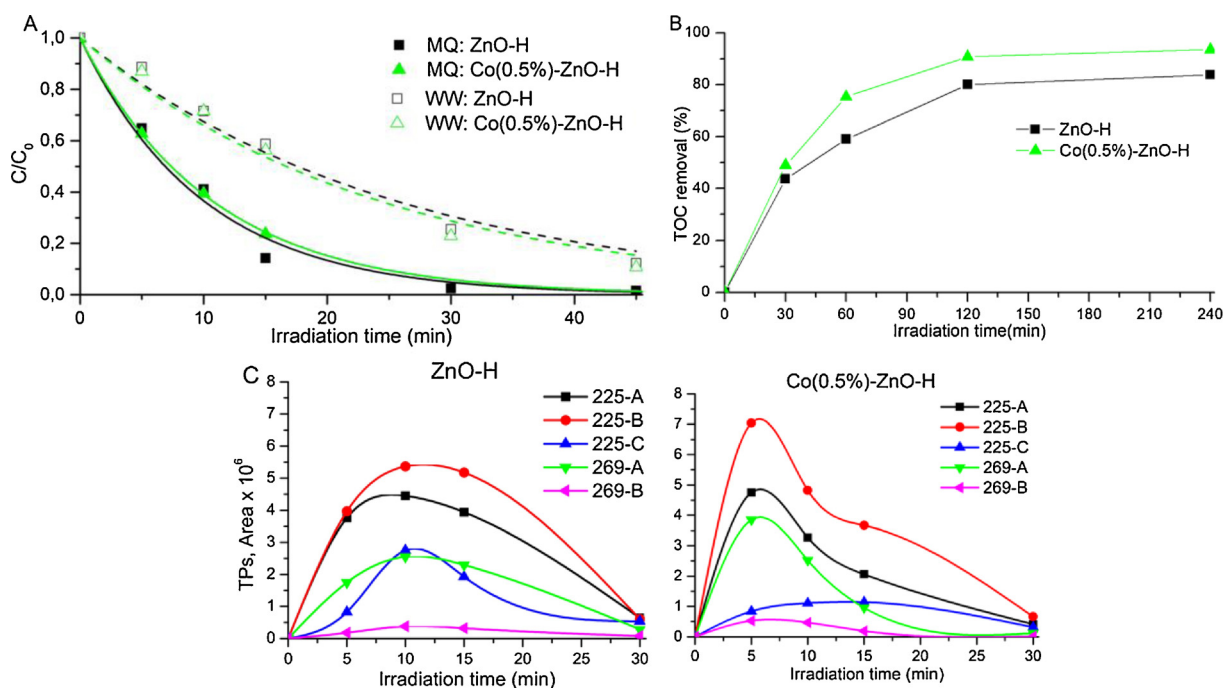


Fig. 8. A) Ketoprofen degradation over time (20 mg/L) under UVA irradiation in the presence of (1000 mg/L) Co(0.5%)-ZnO-H and ZnO-H in Milli-Q water (MQ) and in real wastewater sample (WW). B) TOC removal in during ketoprofen degradation in the presence of ZnO-H and Co(0.5%)-ZnO-H in Milli-Q water. C) Ketoprofen transformation products over time observed in the presence of ZnO-H and Co(0.5%)-ZnO-H.

concentration of TOC. The degradation profiles in Milli-Q water shown in Fig. 8A allow to observe a similar ketoprofen degradation for both doped and pristine zinc oxide. However, the doped material allows to obtain a fast ketoprofen mineralization as shown in Fig. 8B. In fact, Co (0.5%)-ZnO-H is able to reduce ~80% of TOC after 1 h under irradiation while less than 60% was observed for the bare material in the same period.

The evolution profiles of the TPs identified by LC/MS are plotted in Fig. 8C. The TPs present a faster fade with Co-doped ZnO when compared with the bare material. In fact, the TPs maximum concentration is achieved in just 5 min of irradiation for the doped material while longer irradiation times are required for the bare ZnO. The observed ketoprofen TPs were the same described on experiments performed with TiO<sub>2</sub> as shown in Table S1 [47–49].

To study the complexity effect of water matrix composition the ketoprofen degradation was also performed in spiked a real wastewater sample, Fig. 8. The reducing on the degradation efficiency can be attributed to the presence of the inorganic water constitutes and organic matter [50]. Even though, both materials were able to complete abate the pollutant in 1 h of irradiation.

#### 4. Conclusions

Synthesis of cobalt doped ZnO and TiO<sub>2</sub> following different synthetic strategies, namely solution and hydrothermal, led to the materials with distinct morphology and photocatalytic properties. The TiO<sub>2</sub> doped with low amounts (0.25% and 0.5%) prepared by hydrothermal method leads to an enhancement on the phenol degradation comparing to the pristine material. However, if prepared by solution method an inhibition on the photocatalytic activity was observed.

The hydrothermal method proved to be the most advantageous to prepare Co-doped ZnO materials for photocatalytic applications. Doping concentration presents a clear contribution on the material performance, being the one prepared by the addition of 0.5% the most effective on the pollutant model molecule removal. The cobalt ions on ZnO lattice, if in appropriate quantities can act as a trap for the photo-produced charges reducing the electron/hole recombination.

The best performing material was also able to remove ketoprofen in real a wastewater sample, proving to be more efficient on ketoprofen mineralization.

#### Declaration of Competing Interest

The authors declare that they have no known competing financial interests or personal relationships that could have appeared to influence the work reported in this paper

#### Acknowledgments

This work is part of a project that has received funding from the European Union's Horizon 2020 research and innovation programme under the Marie Skłodowska-Curie Grant Agreement No 765860 (AQUALity), moreover, thanks to the contribution of Compagnia di San Paolo supplied under the Multi-Year Convention (2016–2018) between the University of Turin and Compagnia di San Paolo.

#### Appendix A. Supplementary data

Supplementary material related to this article can be found, in the online version, at doi:<https://doi.org/10.1016/j.jece.2019.103475>.

#### References

- [1] S.D. Richardson, T.A. Ternes, Water analysis: emerging contaminants and current issues, *Anal. Chem.* 90 (2018) 398–428.
- [2] M. Taheran, M. Naghdi, S.K. Brar, M. Verma, R.Y. Surampalli, Emerging

- contaminants: Here today, there tomorrow!, *Environ. Nanotechnol., Monit. Manag.* 10 (2018) 122–126.
- [3] A. Gogoi, P. Mazumder, V. Kumar, G.G.T. Chaminda, A. Kyoungjin, M. Kumar, Occurrence and fate of emerging contaminants in water environment: a review, *Groundw. Sustain. Dev.* 6 (2018) 169–180.
- [4] J. Wilkinson, P.S. Hooda, J. Barker, S. Barton, J. Swinden, Occurrence, fate and transformation of emerging contaminants in water: an overarching review of the field, *Environ. Pollut.* 231 (2017) 954–970.
- [5] E. Kudlek, Decomposition of contaminants of emerging, *Water* 10 (2018) 2–18.
- [6] G. Lofrano, G. Libralato, J. Brown, Nanotechnologies for Environmental Remediation: Applications and Implications, (2017).
- [7] M. Salimi, A. Esrafil, M. Gholami, A. Jonidi Jafari, R. Rezaei Kalantary, M. Farzadkia, M. Kermani, H.R. Sobhi, Contaminants of emerging concern: a review of new approach in AOP technologies, *Environ. Monit. Assess.* 189 (2017).
- [8] S.S.A. Bhattacharya, Drinking water contamination and treatment techniques, *Appl. Water Sci.* 7 (2017) 1043–1067.
- [9] C. Byrne, G. Subramanian, S.C. Pillai, Recent advances in photocatalysis for environmental applications, *J. Environ. Chem. Eng.* 6 (2018) 3531–3555.
- [10] K. Nakata, A. Fujishima, TiO<sub>2</sub> photocatalysis: design and applications, *J. Photochem. Photobiol. C Photochem. Rev.* 13 (2012) 169–189.
- [11] V.A. Sakkas, M. Sarro, M. Kalaboka, V. Santoro, T. Albanis, P. Calza, C. Medana, Evaluating the photocatalytic treatment of stevioside by TiO<sub>2</sub> in different aqueous matrices and identification of transformation products, *Sci. Total Environ.* 607–608 (2017) 568–577.
- [12] C. Gionco, D. Fabbri, P. Calza, M.C. Paganini, Synthesis, characterization, and photocatalytic tests of N-doped zinc oxide: a new interesting photocatalyst, *J. Nanomater.* 2016 (2016) 1–7.
- [13] P. Calza, C. Gionco, M. Giletta, M. Kalaboka, V.A. Sakkas, T. Albanis, M.C. Paganini, Assessment of the abatement of acelsulfame K using cerium doped ZnO as photocatalyst, *J. Hazard. Mater.* 323 (2017) 471–477.
- [14] V. Etacheri, C. Di Valentin, J. Schneider, D. Bahnemann, S.C. Pillai, Visible-light activation of TiO<sub>2</sub> photocatalysts: advances in theory and experiments, *J. Photochem. Photobiol. C Photochem. Rev.* 25 (2015) 1–29.
- [15] Y. Lu, Y. Lin, D. Wang, L. Wang, T. Xie, T. Jiang, A high performance cobalt-doped ZnO visible light photocatalyst and its photogenerated charge transfer properties, *Nano Res.* 4 (2011) 1144–1152.
- [16] M.C. Paganini, A. Giorini, N.P.F. Gonçalves, C. Gionco, A. Bianco Prevot, P. Calza, New insight into zinc oxide doped with iron and its exploitation to pollutants abatement, *Catal. Today* (2018).
- [17] M.R.D. Khaki, M.S. Shafeeyan, A.A.A. Raman, W.M.A.W. Daud, Application of doped photocatalysts for organic pollutant degradation - a review, *J. Environ. Manage.* 198 (2017) 78–94.
- [18] N. Geetha, S. Sivarajani, A. Ayeshamariam, J.S. Kissinger, M. Valan Arasu, M. Jayachandran, ZnO doped oxide materials: mini review, *fluid mech. Open Access.* 03 (2016) 1–6.
- [19] K.M. Lee, C.W. Lai, K.S. Ngai, J.C. Juan, Recent developments of zinc oxide based photocatalyst in water treatment technology: a review, *Water Res.* 88 (2016) 428–448.
- [20] F. Huang, A. Yan, H. Zhao, Influences of doping on photocatalytic properties of TiO<sub>2</sub> photocatalyst, in: *semicond. Photocatal. - Mater. Mech. Appl.* (2016) 31–80.
- [21] C. Dhandapani, R. Narayanasamy, S.N. Karthick, K.V. Hemalatha, S. Selvam, P. Hemalatha, M.S. kumar, S.D. Kirupha, H.J. Kim, Drastic photocatalytic degradation of methylene blue dye by neodymium doped zirconium oxide as photocatalyst under visible light irradiation, *Optik (Stuttg.)* 127 (2016) 10288–10296.
- [22] A. Šutka, T. Käämbre, R. Pärna, I. Juhneva, M. Maiorov, U. Joost, V. Kisand, Co doped ZnO nanowires as visible light photocatalysts, *Solid State Sci.* 56 (2016) 54–62.
- [23] K. Jug, V.A. Tikhomirov, Comparative studies of cation doping of ZnO with Mn, Fe, and Co<sup>+</sup>, *J. Phys. Chem. A* 113 (2009) 11651–11655.
- [24] Y. Il Kim, R. Seshadri, Optical properties of cation-substituted zinc oxide, *Inorg. Chem.* 47 (2008) 8437–8443.
- [25] Y. Kumar, A. Sahai, S.F. Olive-Méndez, N. Goswami, V. Agarwal, Morphological transformations in cobalt doped zinc oxide nanostructures: effect of doping concentration, *Ceram. Int.* 42 (2016) 5184–5194.
- [26] A.J. Ebele, M. Abou-Elwafa Abdallah, S. Harrad, Pharmaceuticals and personal care products (PPCPs) in the freshwater aquatic environment, *Emerg. Contam.* 3 (2017) 1–16.
- [27] W.W.P. Lai, Y.C. Lin, H.H. Tung, S.L. Lo, A.Y.C. Lin, Occurrence of pharmaceuticals and perfluorinated compounds and evaluation of the availability of reclaimed water in Kinmen, *Emerg. Contam.* 2 (2016) 135–144.
- [28] E. Cerrato, C. Gionco, I. Berruti, F. Sordello, P. Calza, M.C. Paganini, Rare earth ions doped ZnO: synthesis, characterization and preliminary photoactivity assessment, *J. Solid State Chem.* 264 (2018) 42–47.
- [29] E. Cerrato, C. Gionco, M.C. Paganini, E. Giamello, Photoactivity properties of ZnO doped with cerium ions: an EPR study, *J. Phys. Condens. Matter* 29 (2017) 444001–444007.
- [30] W. Bousslama, H. Elhouichet, M. Férid, Enhanced photocatalytic activity of Fe doped ZnO nanocrystals under sunlight irradiation, *Optik (Stuttg.)* 134 (2017) 88–98.
- [31] P. A.L., The Scherrer Formula for X-Ray Particle Size Determination, *Phys. Rev.* 56 (1939) 978–982.
- [32] V. Yashpal, B.V. Sharma, Manoj Kumar, Issues in determining size of nano-crystalline Ceramic Particles by X-ray diffraction, *Mater. Today Proc.* 2 (2015) 3534–3538.
- [33] C.C. Ding, S.Y. Wu, L.N. Wu, Y.Q. Xu, L.J. Zhang, The investigation of the defect structures for Co<sup>2+</sup> in ZnO microwires, thin films and bulks, *J. Phys. Chem. Solids*

- 106 (2017) 94–98.
- [34] O. Raita, A. Popa, D. Toloman, M. Stan, A. Darabont, L. Giurgiu,  $\text{Co}^{2+}$  Ions in ZnO powders as seen by Magnetic Resonance, *Appl. Magn. Reson.* 40 (2011) 245–250.
- [35] P. Jakes, E. Erdem, Finite size effects in ZnO nanoparticles: An electron paramagnetic resonance (EPR) analysis, *Phys. Status Solidi - Rapid Res. Lett.* 5 (2011) 56–58.
- [36] S.K.S. Parashar, B.S. Murty, S. Repp, S. Weber, E. Erdem, Investigation of intrinsic defects in core-shell structured ZnO nanocrystals, *J. Appl. Phys.* 111 (2012) 1–7.
- [37] E. Cerrato, C. Gionco, M.C. Paganini, E. Giamello, E. Albanese, G. Pacchioni, Origin of visible light photoactivity of the  $\text{CeO}_2/\text{ZnO}$  heterojunction, *ACS Appl. Energy Mater.* 1 (2018) 4247–4260.
- [38] A. Savoyant, H. Alnoor, O. Pilone, O. Nur, M. Willander, Core-defect reduction in ZnO nanorods by cobalt incorporation, *Nanotechnology* 28 (2017) 1–7.
- [39] H. Liu, B. Shen, M. Xing, J. Zhang, B. Tian, Vacuum-activated  $\text{Co}^{2+}$  and  $\text{Ti}^{3+}$  co-modified  $\text{TiO}_2$  with stable and enhanced photocatalytic activity, *Res. Chem. Intermed.* 42 (2016) 3459–3471.
- [40] A. Fujishima, X. Zhang, D.A. Tryk,  $\text{TiO}_2$  photocatalysis and related surface phenomena, *Surf. Sci. Rep.* 63 (2008) 515–582.
- [41] M.A. Henderson, A surface science perspective on  $\text{TiO}_2$  photocatalysis, *Surf. Sci. Rep.* 66 (2011) 185–297.
- [42] M.M. Ba-Abbad, M.S. Takriff, A. Benamor, A.W. Mohammad, Synthesis and characterisation of  $\text{Co}^{2+}$ -incorporated ZnO nanoparticles prepared through a sol-gel method, *Adv. Powder Technol.* 27 (2016) 2439–2447.
- [43] O. Altintas Yildirim, H. Arslan, S. Sönmezoglu, Facile synthesis of cobalt-doped zinc oxide thin films for highly efficient visible light photocatalysts, *Appl. Surf. Sci.* 390 (2016) 111–121.
- [44] Z. Guo, R. Ma, G. Li, Degradation of phenol by nanomaterial  $\text{TiO}_2$  in wastewater, *Chem. Eng. J.* 119 (2006) 55–59.
- [45] T.T.T. Dang, S.T.T. Le, D. Channei, W. Khanitchaidecha, A. Nakaruk, Photodegradation mechanisms of phenol in the photocatalytic process, *Res. Chem. Intermed.* 42 (2016) 5961–5974.
- [46] A. Jelic, M. Gros, A. Ginebreda, R. Cespedes-Sánchez, F. Ventura, M. Petrovic, D. Barcelo, Occurrence, partition and removal of pharmaceuticals in sewage water and sludge during wastewater treatment, *Water Res.* 45 (2011) 1165–1176.
- [47] C. Martínez, S. Vilariño, M.I. Fernández, J. Faria, M.L. Canle, J.A. Santaballa, Mechanism of degradation of ketoprofen by heterogeneous photocatalysis in aqueous solution, *Appl. Catal. B Environ.* 142–143 (2013) 633–646.
- [48] A. Jakimska, M. Śliwka-Kaszyńska, J. Reszczyńska, J. Namieśnik, A. Kot-Wasik, Elucidation of transformation pathway of ketoprofen, ibuprofen, and furosemide in surface water and their occurrence in the aqueous environment using UHPLC-QTOF-MS Euroanalysis XVII, *Anal. Bioanal. Chem.* 406 (2014) 3667–3680.
- [49] R.K. Szabó, C.S. Megyeri, E. Illés, K. Gajda-Schranz, P. Mazellier, A. Dombi, Phototransformation of ibuprofen and ketoprofen in aqueous solutions, *Chemosphere* 84 (2011) 1658–1663.
- [50] N. Rioja, S. Zorita, F.J. Peñas, Effect of water matrix on photocatalytic degradation and general kinetic modeling, *Appl. Catal. B Environ.* 180 (2016) 330–335.